Dalton Transactions

Accepted Manuscript

ROYAL SOCIETY OF CHEMISTRY

www.rsc.org/dalton

Journal Name

RSCPublishing

ARTICLE

A Single Probe to Sense Al(III) Colorimetrically and Cd(II) by Turn-On Fluorescence in Physiological Conditions and Live Cells: Corroborated by X-ray crystallographic and Theoretical studies

Cite this: DOI: 10.1039/x0xx00000x

Received 00th January 2012,
Accepted 00th January 2012

DOI: 10.1039/x0xx00000x

www.rsc.org/

Chirantan Kar[a], Soham Samanta[a], Sudeep Goswami[b], Aiyagari Ramesh[*b] and Gopal Das[*a]

A pyridine-2-carbohydrazide functionalized conjugated fluorophoric Schiff base ligand $\mathbf{L_1}$ specifically sense Al^{3+} and Cd^{2+} ions through significant changes in their absorption and emission spectral behavior, respectively, in physiological condition. The spectral changes are in the visible region of the spectrum and thus facilitate naked eye detection. Apart from the visible changes, an in-field device application was demonstrated by sensing these ions in paper strips coated with $\mathbf{L_1}$. The crystal structure of the $\mathbf{L_1}$-**Cd** complex provided additional insight of the metal coordination attribute of $\mathbf{L_1}$. Interestingly, fluorescence microscopic studies demonstrated that the ligand $\mathbf{L_1}$ could also be used as an effective probe in imaging experiments for detection of intracellular Cd^{2+} ions in HeLa cells without any toxicity to these model human cells.

Introduction

Chemosensors for selective detection of various biologically and environmentally important metal ions have recently attracted great attention. Among various heavy metal ions cadmium ions are banned in electrical and electronic equipment by the European Union's Restriction on Hazardous Substances (RoHS) directive due to their adverse effect to human health.[1] Cadmium metal ion is also not biodegradable, thus can be easily accumulated in the environment, resulting in contaminated food and water.[2] Cadmium is also an extremely toxic and carcinogenic metal.[3] Although intake of cadmium may also take place through smoking and food, but inhalation of cadmium-containing dust is the major route. Cadmium is generally found in electric batteries, pigments in plastics, electroplated steel, and so on.[4] A high exposure level of cadmium is related to damage of liver and kidneys, increased risks of cardiovascular diseases, and cancer mortality. Therefore, cadmium was listed as number 7 on ATSDR's "CERCLA Priority List of Hazardous Substances"[5] and may cause acute and chronic toxicity.

In fact, there are some fluorescent sensors that have been recently reported for detection and analysis of cadmium metal ions.[6] However, there are only a few fluorescent sensors that can detect cadmium with a fluorescence signal at higher wavelength (orange or red) region of the spectra,[6] and even rare examples are available in living cells.[7] So far, the greatest challenge for detecting Cd^{2+} comes from the interference of other transition metal ions like Zn^{2+}, as they are in the same group of the periodic table and hence exhibit similar chemical properties. This sensing impediment underscores the need for developing Cd^{2+}-selective sensors that can distinguish Cd^{2+} from Zn^{2+} with high sensitivity and selectivity under physiological conditions.

Along with cadmium, aluminium is also one of the most biologically and environmentally relevant metal. Aluminium is the third most abundant element (after oxygen and silicon), and the most abundant metal, in the Earth's crust. Aluminium is generally found in most animal and plant tissues and in natural waters in its ionic form Al^{3+}. Frequent use of aluminium in water treatment, food additive, pharmaceutical products, occupational dusts and cooking utensils results in moderate increase in the Al^{3+} concentration in food. Tolerable weekly aluminium dietary intake in the human body is estimated to be 7 mg/kg body weight.[8] After absorption Al^{3+} is carried by the plasma proteins and distributed in all tissues of human and animals and eventually accumulate in bone, causing softening of the bone, atrophy, and even aberrance.[9] The presence of Al^{3+} ions have been implicated in the damage of the central nervous system and is also thought to be involved in neurodegenerative ailments such as Alzheimer's disease and Parkinson's syndrome.[9] Considering the physiological relevance and biomedical implications of Al^{3+}, there is significant interest in developing selective and sensitive Al^{3+} sensors. Until recently, only a few fluorescent chemosensors have been developed for detection of Al^{3+}.[10-13]

In recent years, fluorescent chemosensors have attracted significant interest because of their potential use in medicinal and environmental research. The most commonly employed method used for metal ion detection is the designing of ligand molecule containing an electron donating group at one end and a metal coordination site at the other end, binding of metal ions

to the ligand initiate the flow of electron from the electron donating site through conjugated pi electron system, which is accompanied by an observable change in the electronic or fluorescence spectra of the ligand.

Most fluorescent sensors for Al^{3+} as well as Cd^{2+} possess good selectivity, but demonstration of these sensor for in-field device application are scarcely reported. In our continuous endeavour to develop sensor for various analytes, [14] herein, we demonstrate the cadmium and aluminium sensing capabilities of a pyridine-2-carbohydrazide functionalized conjugated fluorophoric Schiff base ligand $\mathbf{L_1}$ (Scheme 1) and the absorption and fluorescence behaviour of $\mathbf{L_1}$ upon metal complexation. The strong selectivity and in-field application possibility of the developed sensor is verified by using it in paper strips. We have also demonstrated that the developed sensor as well as the ligand-cadmium complex was non-toxic and the ligand $\mathbf{L_1}$ could readily detect the presence of intracellular Cd^{2+} ions in live HeLa cells via a characteristic fluorescence switch ON mechanism.

Experimental section

General information and materials

All the materials for synthesis were purchased from commercial suppliers and used without further purification. The absorption spectra were recorded on a Perkin-Elmer Lamda-750 UV-visible spectrophotometer using 10 mm path length quartz cuvettes in the range of 300–800 nm wavelengths, while the fluorescence measurements were carried on a Horiba Fluoromax-4 spectrofluorometer using 10 mm path length quartz cuvettes with a slit width of 5 nm at 298 K. NMR spectra were recorded using Bruker 600 MHz instrument and Varian FT-400 MHz instrument. The mass spectra of $\mathbf{L_1}$, $\mathbf{L_1}$**-Cd** and $\mathbf{L_1}$**-Al** complex was obtained using Waters Q-ToF Premier mass spectrometer. The chemical shifts were recorded in parts per million (ppm) on the scale. The following abbreviations are used to describe spin multiplicities in ^{1}H NMR spectra: s = singlet; d = doublet; t = triplet; m= multiplate. Elemental analyses were performed with a Perkin Elmer 2400 elemental analyzer.

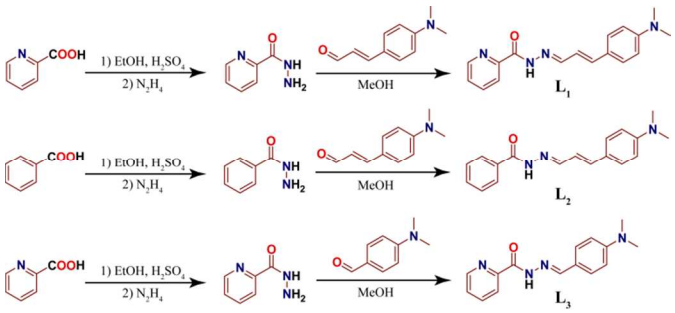

Scheme 1 Synthetic scheme for the ligand L_1, L_2 and L_3

Synthesis of L_1

Picolinohydrazide was prepared following a literature method.[15] Picolinohydrazide (137 mg, 5 mmol) and 4-(Dimethylamino)cinnamaldehyde (175 mg, 5 mmol) were dissolved in 5 mL of methanol. To this was added approximately 2 drops of acetic acid, and the resulting solution was stirred at room temperature for 10 h. A yellow precipitate was obtained, which was collected through filtration. The residue was washed thoroughly with methanol to isolate $\mathbf{L_1}$ in pure form with 68% yield (the yield was calculated based on the starting reagents). ^{1}H NMR [600 MHz, $CDCl_3$, $SiMe_4$, J (Hz), δ (ppm)]: 10.81 (1H, s), 8.55 (1H, d, j=4.2), 8.29 (1H, d, J=8.4), 7.98 (1H, d, J=9), 7.86-7.89 (1H, m), 7.45-7.47 (1H, m), 7.36 (2H, d, J=9), 6.96 (1H, q, J=9, J=15.6), 6.85 (1H, d, J=15.6), 6.67 (2H, d, J=8.4), 2.99 (6H, s,). ^{13}C NMR [150 MHz, $CDCl_3$, $SiMe_4$, δ (ppm)]: 159.99, 151.51, 151.21, 149.41, 148.17, 141.22, 137.71, 128.78, 126.72, 124.08, 123.02, 120.54, 112.24, 40.36. ESI-MS (positive mode, m/z). Calcd for $C_{17}H_{18}N_4O$: 294.148. Found: 295.155 (M + H^+). Anal. Calcd. for $C_{17}H_{18}N_4O$ (294.15): C 69.13, H 6.48, N 18.97, O 5.42; found C 69.10, H 6.45, N 19.08, O 5.37.

Synthesis of L_2

Benzohydrazide was prepared following a literature method.[16] Benzohydrazide (136 mg, 5 mmol) and 4-(Dimethylamino)cinnamaldehyde (175 mg, 5 mmol) were dissolved in 5 mL of methanol. To this was added approximately 2 drops of acetic acid, and the resulting solution was stirred at room temperature for 10 h. A yellow precipitate was obtained, which was collected through filtration. The residue was washed thoroughly with methanol to isolate $\mathbf{L_2}$ in pure form with 82% yield (the yield was calculated based on the starting reagents). ^{1}H NMR [400 MHz, DMSO-d_6, J (Hz), δ (ppm)]: 11.61 (1H, s), 8.18 (1H, d, j=8.8), 7.89 (2H, d, j=7.6), 7.57 (1H, d, j=6.8), 7.51 (2H, t, j=6.8), 7.45 (2H, d, j=8.4), 6.91 (1H, d, j=16), 6.78 (1H, q, j=9.2, j=15.6), 6.70 (2H, d, j=8), 2.94 (6H, s). ^{13}C NMR [100 MHz, DMSO-d_6, δ (ppm)]: 162.75, 150.74, 139.87, 133.67, 131.56, 128.44, 127.57, 123.68, 120.56, 112.03, 40.20. ESI-MS (positive mode, m/z). Calcd for $C_{18}H_{19}N_3O$: 293.153. Found: 294.161 (M + H^+). Anal. Calcd. for $C_{18}H_{19}N_3O$ (293.153): C 73.44, H 6.85, N 14.27, O 5.44; found C 73.40, H 6.83, N 14.40, O 5.37.

Synthesis of L_3

$\mathbf{L_3}$ was synthesized following a method previously reported in literature.[17]

Synthesis of Cadmium complex for crystallization

A solution of $\mathbf{L_1}$ in DMF was stirred and refluxed in presence of 1 equivalent of Cadmium chloride. The color of the solution changes to dark yellow after addition of the cadmium salt. The stirring is continued in reflux condition for 2 hours until the solution color changed to dark reddish. The resulting solution was cooled, filtered and kept for crystallization. ^{1}H NMR [400 MHz, DMSO-d_6, J (Hz), δ (ppm)]: 12.08 (1H, s), 8.69 (1H, s), 8.37 (1H, d, j=8.8), 8.10 (1H, d, j=7.6), 8.04 (1H, t, j=7.2), 7.65 (1H, s), 7.43 (2H, d, j=8.4), 6.92 (1H, d, j=16), 6.81 (1H, d, j=8.8), 6.70 (2H, d, j=7.6) 2.50 (6H, s). ESI-MS (positive mode, m/z). Calcd for $(C_{17}H_{19}N_4O)_2CdCl_2$: 774.152. Found: 737.163 $[(C_{17}H_{19}N_4O)_2CdCl]^+$.

UV−Vis and fluorescence spectral studies

Stock solutions of various ions (1×10^{-3} mol·L^{-1}) were prepared in deionized water. A stock solution of $\mathbf{L_1}$ (1×10^{-3} mol·L^{-1}) was prepared in DMSO. The solution of $\mathbf{L_1}$ was then diluted to 1×10^{-5} mol·L^{-1} with CH_3OH/aqueous HEPES buffer (5 mM, pH 7.3; 1:4 v/v). In each titration experiments a 1×10^{-3} L solution of $\mathbf{L_1}$ (1×10^{-5} mol·L^{-1}) was taken in a quartz optical cell of 1 cm optical path length, and then the ion

stock solutions were added into the optical cell gradually by using a micropipette. Spectral data were recorded at 1 min after the addition of the ions. In selectivity experiments, the test samples were prepared by placing appropriate amounts of the cations stock into 2 mL of solution of $\mathbf{L_1}$ (2×10^{-5} mol·L^{-1}). For fluorescence measurements, excitation was provided at 405 nm, and emission was collected from 420 to 750 nm.

Evaluation of the binding constant for the formation of $L_1 \cdot Cd^{2+}$ and $L_1 \cdot Al^{3+}$

Receptor $\mathbf{L_1}$ with an effective concentration of 10.0×10^{-6} M in a Methanol/aqueous HEPES buffer (5 mM; 1:4, v/ v; pH 7.3) was used for the spectroscopic titration studies with a Cd^{2+} or Al^{3+} solution. A stock solution of $Cd(NO_3)_2$ or $Al(NO_3)_3$, having a concentration of 0.2×10^{-3} M in an Methanol/aqueous HEPES buffer (1:4, v/v; pH 7.3) solution was used. The effective Cd^{2+} or Al^{3+} concentration was varied between 0 and 5×10^{-5} M for this titration. The solution pH was adjusted to 7.3 using an aqueous HEPES buffer solution having an effective concentration of 5 mM.

Binding constants using spectroscopic titration data

The binding constant for the formation of the respective complexes were evaluated using the Benesi−Hildebrand (B−H) plot (eq 1 and eq 2).[18]

$$1/(A-A_0)=1/\{K(A_{max}-A_0)C\}+1/(A_{max}-A_0) \quad (1)$$

$$1/(I-I_0)=1/\{K(I_{max}-I_0)C\}+1/(I_{max}-I_0) \quad (2)$$

A_0 is the absorbance of $\mathbf{L_1}$ at absorbance maximum (λ = 510 nm), A is the observed absorbance at that particular wavelength in the presence of a certain concentration of the metal ion (C), A_{max} is the maximum absorbance value that was obtained at λ = 510 nm during titration with varying metal ion concentration, K is the binding constant (M^{-1}) and was determined from the slope of the linear plot, and C is the concentration of the Al^{3+} ion added during titration studies.

I_0 is the emission intensity of $\mathbf{L_1}$ at emission maximum (λ = 578 nm), I is the observed emission intensity at that particular wavelength in the presence of a certain concentration of the metal ion (C), I_{max} is the maximum emission intensity value that was obtained at λ = 578 nm during titration with varying metal ion concentration, K is the binding constant (M^{-1}) and was determined from the slope of the linear plot, and C is the concentration of the Cd^{2+} ion added during titration studies.

Detection limit for Cd^{2+} and Al^{3+}

The detection limit was calculated based on the UV-Vis titration for Cd^{2+} and fluorescence emission in case of Al^{3+}. The fluorescence emission spectrum of $\mathbf{L_1}$ was measured ten times and the standard deviation of blank measurement was achieved. To gain the slop, the UV-Vis absorbance (or fluorescence emission in case of Cd^{2+}) at 510 nm (or at 578 nm in case of Cd^{2+}) and was plotted as a concentration of the corresponding metal ion concentration. The detection limit was calculated with the following equation:

Detection limit = $3\sigma/k$

Where σ is the standard deviation of blank measurement, k is the slop between the ratio of UV-Vis absorbance (or fluorescence emission) versus metal ion concentration.

X-ray Crystallography

In each case, a crystal of suitable size was selected from the mother liquor and immersed in silicone oil, and it was mounted on the tip of a glass fibre and cemented using epoxy resin. The intensity data were collected using a Bruker SMART APEXII CCD diffractometer, equipped with a fine-focus 1.75 kW sealed-tube Mo Kα radiation (λ = 0.710 73 Å) at 298(3) K, with increasing ω (width of 0.3° frame^{-1}) at a scan speed of 5 s frame^{-1}. SMART software was used for data acquisition. Data integration and reduction were undertaken with SAINT and XPREP[19] software. Multiscan empirical absorption corrections were applied to the data using the program SADABS.[20] Structures were solved by direct methods using SHELXS-97[21] and refined with full-matrix least squares on F^2 using SHELXL-97.[22] All non-hydrogen atoms were refined anisotropically. The hydrogen atoms were located from the difference Fourier maps and refined. Structural illustrations have been drawn with ORTEP-3 for Windows.[23]

Table 1. Crystallographic Parameters and Refinement Details of $\mathbf{L_1}$ and $\mathbf{L_1}$-**Cd** Complex

Parameters	$\mathbf{L_1}$	$\mathbf{L_1}$-Cd
Formula	$C_{17}H_{18}N_4O$	$C_{34}H_{40}CdCl_2N_8O_4$
Formula weight	294.35	808.05
Crystal system	Monoclinic	Monoclinic
Space group	P21	C2/c
a (Å)	5.9895(4)	18.0309(4)
b (Å)	14.7978(8)	10.7197(4)
c (Å)	17.8142(14)	20.3059(6)
β (deg)	96.481(6)	111.574(2)
V (Å)	1568.81(18)	3649.88(19)
Z	4	4
T (K)	298(2)	298(2)
μ (cm^{-1})	0.081	0.793
d_{cal} (g cm^{-3})	1.246	1.470
crystal dimens (mm^3)	0.25×0.16×0.14	0.26×0.20×0.16
no. of reflns collected	2513	3086
no. of unique reflns	5103	4158
no. of params	401	236
R1; wR2 (I>2σ(I))	0.0776; 0.2489	0.0308;0.0958
R1; wR2(all)	0.1564; 0.3180	0.0422; 0.1066
GOF (F2)	0.932	0.783
CCDC No.	989403	989402

Computational Methods

Full geometry optimizations were carried out using the density functional theory (DFT) method at the Becke-3-Lee-Yang-Parr (B3LYP)[24] level for the ligand $\mathbf{L_1}$ and its octahedral Al^{3+} complexes (for both the possibilities; 'N' coordinated and 'O' coordinated). The 6-31+G (d,p) basis set was assigned for all the elements. All calculations were performed with Gaussian03 program with the aid of the GaussView visualization program.

Cytotoxic effect on HeLa cells

The cytotoxic potential of compound $\mathbf{L_1}$ and $\mathbf{L_1}$-**Cd** complex was ascertained by an MTT assay following the manufacturer instruction (Sigma-Aldrich, MO, USA). HeLa cells were initially propagated in a 25 cm^2 tissue culture flask in Dulbecco's Modified Eagle Medium (DMEM) supplemented with 10% (v/v) fetal bovine serum (FBS), penicillin (100 μg/mL) and streptomycin (100 μg/mL) in a CO_2 incubator. Prior to MTT assay, cells were seeded into 96-well plates (approximately 10^4 cells per well) and various concentrations of compound $\mathbf{L_1}$ and $\mathbf{L_1}$-**Cd** complex (15, 30, 45 and 60 μM) made

in DMEM were added to the cells and incubated for 24 h. Solvent control samples (cells treated with DMSO alone) and cells treated with $Cd(NO_3)_2$ alone were also included in parallel sets. Following incubation, the growth media was removed and fresh DMEM containing MTT solution was added. The plate was incubated for 3-4 h at 37°C. Subsequently, the supernatant was removed and the insoluble colored formazan product was solubilized in DMSO and its absorbance was measured in a microtitre plate reader (Infinite M200, TECAN, Switzerland) at 550 nm. The assay was performed in six sets for each concentration of compound **L_1** and **L_1-Cd** complex. Data analysis and calculation of standard deviation was performed with Microsoft Excel 2010 (Microsoft Corporation, USA). For statistical analysis, a one way analysis of variance (ANOVA) was performed using Sigma plot.

Cell culture and imaging studies

HeLa cells were initially propagated in a 25 cm^2 tissue culture flask as described earlier and then seeded into a 6 well plate and incubated at 37^0 C in a CO_2 incubator for 3 days. Subsequently the cells were washed three times with sterile phosphate buffered saline (pH 7.4) and incubated with 10 μM **L_1** in DMEM at 37 °C for 1 h in a CO_2 incubator. The image of the cells was then recorded using an epifluorescence microscope (Nikon Eclipse Ti). The cells were again washed thrice with sterile PBS (pH 7.4) to remove excess **L_1**, and then incubated in sterile PBS (pH 7.4) with 20 μM $Cd(NO_3)_2$ for 1 h and the image of the cells were again recorded using epifluorescence microscope.

Results and Discussions

UV-vis spectroscopic studies of L_1 in presence of metal ions

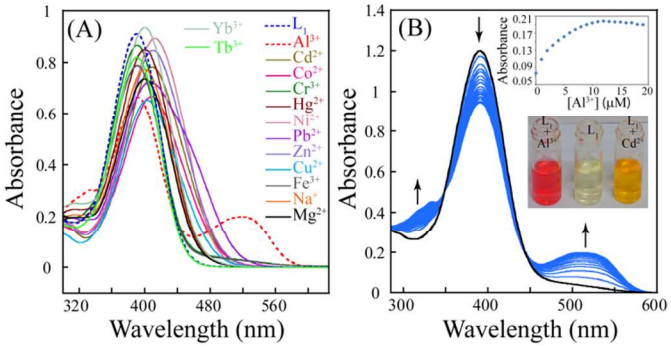

Fig. 1 (A) UV-Vis absorption spectra of receptor **L_1** (10 μM) observed upon addition of 5 equivalent metal ions (perchlorate or nitrate salts of Na^+, Mg^{2+}, Cr^{3+}, Hg^{2+}, Cu^{2+}, Pb^{2+}, Zn^{2+}, Fe^{3+}, Co^{2+}, Ni^{2+}, Cd^{2+}, Yb^{3+}, Tb^{3+} and Al^{3+}) in a CH_3OH/aqueous HEPES buffer (5 mM, pH 7.3; 1:4 v/v). (B) UV-Vis titration spectra of **L_1** (10 μM) upon incremental addition of $Al(NO_3)_3$ in CH_3OH/aqueous HEPES buffer (5 mM, pH 7.3; 1:4 v/v). **Inset:** Changes in the absorbance at 510 nm with incremental addition of Al^{3+} and visual change in the solution colour after addition of metal ions.

UV−vis spectra recorded for **L_1** in CH_3OH/aqueous HEPES buffer (5 mM, pH 7.3; 1:4, v/v) indicated an absorption maximum at 390 nm, which may have originated due to the intra-molecular π-π* charge transfer (CT) transition. The selectivity of **L_1** was verified with perchlorate or nitrate salts of Na^+, Mg^{2+}, Cr^{3+}, Hg^{2+}, Cu^{2+}, Pb^{2+}, Zn^{2+}, Fe^{3+}, Co^{2+}, Ni^{2+}, Cd^{2+}, Yb^{3+}, Tb^{3+} and Al^{3+} in CH_3OH/aqueous HEPES buffer (5 mM, pH 7.3; 1:4 v/v). Although other metal ions like Cd, Ni, Zn, Pb and Co exhibit some binding with the receptor **L_1** which is accompanied by 40 nm red shift of the absorption maxima but a significant change in UV-vis spectral pattern was observed only in presence of Al^{3+}, among all the other metal ions used (Figure 1A). Upon addition of Al^{3+}, the intensity of the absorption bands of **L_1** at 390 nm decreased with a concomitant appearance of two new bands at 330 nm and at 510 nm. The change in the UV-vis spectra is also well supported by a visual change of the receptor solution from yellow to dark red on addition of nearly 1.0 equivalent of Al^{3+} ions (Figure 1B inset). We have also performed the UV-vis titration experiment with incremental amount of Al^{3+} ions, wherein two well-defined isosbestic points at 348 and 445 nm were observed (Figure 1B), which clearly suggested a prominent conversion of **L_1** into the **L_1-Al** complex. The complex formed between **L_1** and Al^{3+} was observed to be 1:1 in stoichiometry, which was established with the help of job's plot (supporting information figure S6) based on the changes in absorbance at 510 nm. This stoichiometry in the solution state was also supported by ESI-MS studies (supporting information figure S7), which indicated the presence of a molecular-ion peak at m/z 445.05, corresponds to the mass of $[\mathbf{L_1}+Al+3Cl+H_2O+H]^+$. The binding constant for the formation of **L_1-Al** complex was also calculated on the basis of change in absorbance at 510 nm by considering a 1:1 binding stoichiometry (supporting information figure S8). The binding constant (*K*) determined by the B-H method was found to be 5×10^4 M^{-1}. It is significant to mention that the detection limit of **L_1** for Al^{3+} ions was found to be 8.7 μM (supporting information figure S9) which is lower than tolerable weekly aluminium dietary intake in an average human body.[8] The selective change in the absorbance spectra of **L_1** can be attributed to the high positive charge of the metal ion. On complexion with **L_1**, Al^{3+} significantly attracts the electron cloud from the N,N dimethyl moiety via conjugated π-electron system and the probability of Internal charge transfer (ICT) also increases resulting in formation of a red shifted new band in the spectra.

For a theoretical appraisal on the selective chromogenic response of **L_1** toward Al^{3+}, the Density Functional Theory Calculation (DFT) of **L_1** and its Aluminium complex were carried out. The electronic spectrum of **L_1** alone showing absorbance maximum at 390 nm is mainly generated from the transition of HOMO to LUMO. However as both the Job's plot and mass spectrum indicated formation of a 1:1 **L_1-Al** complex; we have performed the structure optimization of **L_1-Al** complex to explore the most suitable binding mode between **L_1** and Al^{3+}. As for Al^{3+} two probable coordination sites are available, the first one involving the pyridine nitrogen (Structure **i** in figure 2A) and the second one involving the carbonyl oxygen (structure **ii** in figure 2A), theoretical calculations were done for both the possibility. Structure 'ii' was found to be 8.01 Kcal more stable than structure 'i' (supporting information table S1). Thus it can be argued here that chelation of Al^{3+} with **L_1** involving the carbonyl oxygen and the imine nitrogen led to the formation of a highly stable complex. The DFT calculation revealed that there is a reasonable decrease in the HOMO to LUMO energy gap from **L_1** to its Aluminium complex (figure 2B) which is in agreement with the subsequent generation of the red shifted new absorbance peak on addition of Al^{3+} to **L_1**. The comparison between the structure of **L_1** and **L_1-Al** complex clearly revealed that on chelation with the Al^{3+}, ligand **L_1** gained perfect planarity with an extended conjugation (supporting information figure S10). Thus, undoubtedly the formation of the highly stable **L_1-Al** complex followed by extension in the conjugation and increases in the probability of

charge transfer initiated this unusual colorimetric response. Selected orbitals and their corresponding energies for both **L_1** and **L_1-Al** complex, which are likely to be critical in the optical spectral outcome are provided in supporting information (supporting information table S2 and table S3).

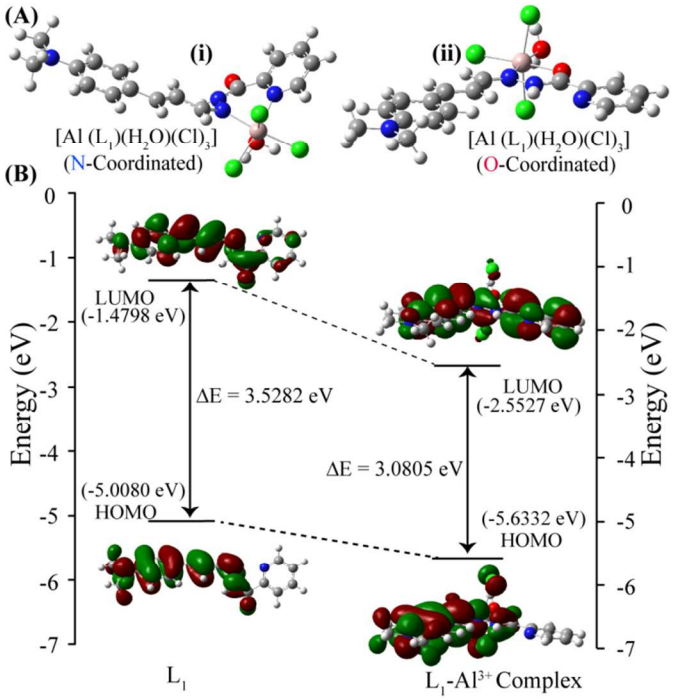

Fig. 2 (A) Optimized structures of **L_1**–Al^{3+} complex with two different possible binding modes. (B) Energy diagrams of HOMO and LUMO orbitals of **L_1** and the **L_1**–Al^{3+} complex (structure **i**) calculated at the DFT level using a B3LYP/6-31+G(d,p) basis set.

Fluorescence spectroscopic studies of L_1 in presence of metal ions

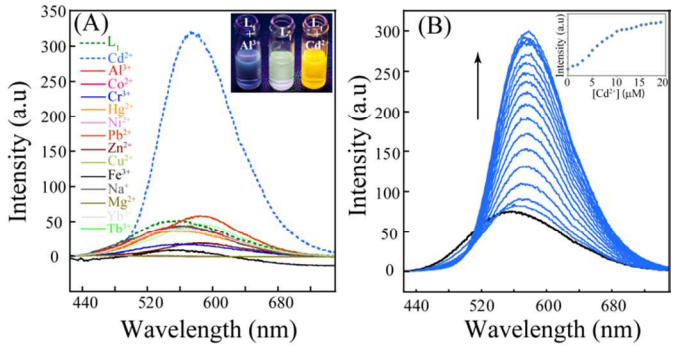

Fig. 3 (A) Changes of the fluorescence emission of receptor **L_1** (10 μM) observed upon addition of 5 equivalent metal ions (perchlorate or nitrate salts of Na^+, Mg^{2+}, Cr^{3+}, Hg^{2+}, Cu^{2+}, Pb^{2+}, Zn^{2+}, Fe^{3+}, Co^{2+}, Ni^{2+}, Cd^{2+}, Yb^{3+}, Tb^{3+} and Al^{3+}) in a CH_3OH/aqueous HEPES buffer (5 mM, pH 7.3; 1:4 v/v). **Inset:** Visual change in the solution fluorescence after addition of metal ions. (B) Fluorescence titration spectra of **L_1** (10 μM) upon incremental addition of $Cd(NO_3)_2$ (upto 2 equuivalent) in CH_3OH/aqueous HEPES buffer (5 mM, pH 7.3; 1:4 v/v). **Inset:** Changes in the emission intensity at 578 nm with incremental addition of Cd^{2+}.

The selectivity of **L_1** for different metal ions (Na^+, Mg^{2+}, Cr^{3+}, Hg^{2+}, Cu^{2+}, Pb^{2+}, Zn^{2+}, Fe^{3+}, Co^{2+}, Ni^{2+}, Cd^{2+}, Yb^{3+}, Tb^{3+} and Al^{3+} in CH_3OH/aqueous HEPES buffer) was also studied by fluorescence emission spectroscopy. As evident from Figure 3A, a solution of **L_1** (10.0×10^{-6} M) exhibited a low intensity emission maxima at 554 nm when excited at 405 nm. Addition of Cd^{2+} to this receptor solution induced a dramatic increase in the fluorescence intensity along with a significant red shift of the emission maxima to 578 nm. The increase in fluorescence was also observed under an UV lamp wherein there was a sharp change in the solution fluorescence from colorless to orange in presence of Cd^{2+} ions (Figure 3A inset)**.** It can also be observed from Figure 3A that the metal-ligand binding induced switch-ON fluorescence of **L_1** was entirely selective towards Cd^{2+} ions, as no significant fluorescence change of **L_1** occurred even in the presence of excess of other metal ions. To further understand the properties of **L_1** as a receptor for Cd^{2+}, a titration of the receptor was performed with increasing concentration of Cd^{2+}. As evident in Figure 3B the fluorescence intensity of a 10 μM solution of **L_1** was enhanced systematically with incremental addition of Cd^{2+} ions, which also confirmed that receptor **L_1** exhibited a high sensitivity toward Cd^{2+}. The 1:1 stoichiometry of the **L_1-Cd** was established from the measurements of emission intensity as a function of Cd^{2+} concentration (inset in Figure 3B), where a clear bend of the curve was observed at 1.0 equivalent of added Cd^{2+}.

This stoichiometry in the solution state was also confirmed with the help of job's plot (supporting information figure S6) and further supported by ESI-MS studies (supporting information figure S13), which indicated the presence of a molecular-ion peak at m/z 443.02, corresponds to the mass of [**L_1** + Cd^{2+} + Cl]. The binding constant for the formation of **L_1-Cd** complex was calculated on the basis of change in emission at 578 nm by considering a 1:1 binding stoichiometry (supporting information figure S7). The binding constant (*K*) determined by the B-H method was found to be 1.6×10^5 M^{-1}. The detection limit of **L_1** for Cd^{2+} ions was found to be 1.2 μM (supporting information figure S9).

The change in emission spectral behavior of **L_1** in presence of Cd^{2+} can be explained by chelation-enhanced fluorescence (CHEF). Although **L_1** is a conjugated system but the metal binding site and the N,N-dimethyl aniline ring of **L_1** may not be perfectly planar in the free ligand. Metal coordination renders the system more planarity which in turn increases the rigidity of the system[25] and consecutively enhances the internal charge transfer from the N,N-dimethyl aniline moiety to the metal binding cites. In absence of the metal ions there is no sufficient pull for the electronic charge over the N, N- Dimethyl substituted benzene ring and thus the fluorescence is quenched due to lack of internal charge transfer throughout the system. But binding of a suitable metal cation by the imine nitrogen and the amide oxygen may drag the electronic charge from the N, N- Dimethyl substituted benzene ring. Due to the metal ion assisted electron pull and the N, N- Dimethyl inducted electron push, the possibility of internal charge transfer throughout the π-system increases; leading to a highly conjugated geometry and a radical enhancement of the fluorescence intensity. To further verify the significance of the conjugated chain length and the pyridine unit in the sensing event of metal ions, we have synthesized two control compounds **L_2** and **L_3**. **L_2** has a similar structure to **L_1** but in place of a pyridine moiety in **L_1** a benzene moiety is present. In case of **L_3** we had chosen N, N dimethyl carboxaldehyde in place of the cinnamaldehyde (Scheme 1). Fluorescence emission and UV-Vis spectroscopic studies with **L_2** and **L_3** revealed some interesting facts, which help us to further understand the beauty of the ligand designing. From fluorescence emission spectra of **L_2** we found that there was no significant increase in the emission intensity with the

tested metal ions, similarly UV-vis absorbance was also almost unchanged upon addition of an excess amount of Cd^{2+}/Al^{3+} to a solution containing $\mathbf{L_2}$ (supporting information figure S14 and figure S15). whereas in case of $\mathbf{L_3}$ there was a significant increase in the emission intensity (at 520 nm) in presence of Cd^{2+}, although the response towards Zn^{2+} ions is much more pronounced but perceivable change in presence of Cd^{2+} is sufficient enough to understand the significance of the pyridine moiety to control the optical response of the ligand towards specific cations. Similar to the result obtained from the fluorescence spectroscopy, UV-Vis absorbance shows formation of a new peak (near 450 nm) in presence of Al^{3+} ions. Thus, from the above mentioned result it can be concluded that the presence of both, the long conjugated geometry as well as the pyridine moiety are significant prerequisites for the metal sensing ability of $\mathbf{L_1}$. The pyridine ring basically controls the selective optical response for the metal ions and the extended conjugation assist to shift the optical response to longer wavelength region of the spectrum. Quantum yield recorded for $\mathbf{L_1}$, $\mathbf{L_2}$, $\mathbf{L_3}$ and $\mathbf{L_1}$ in presence of 1 equivalent of Cd^{2+} ions are 0.08, 0.02, 0.009 and 0.25 respectively. (Quinine sulfate in 0.1N H_2SO_4 was used as the standard for quantum yield measurements).

Further proof of the metal binding modes of the ligand was obtained from the X-ray crystallographic studies of $\mathbf{L_1}$-**Cd** complex.

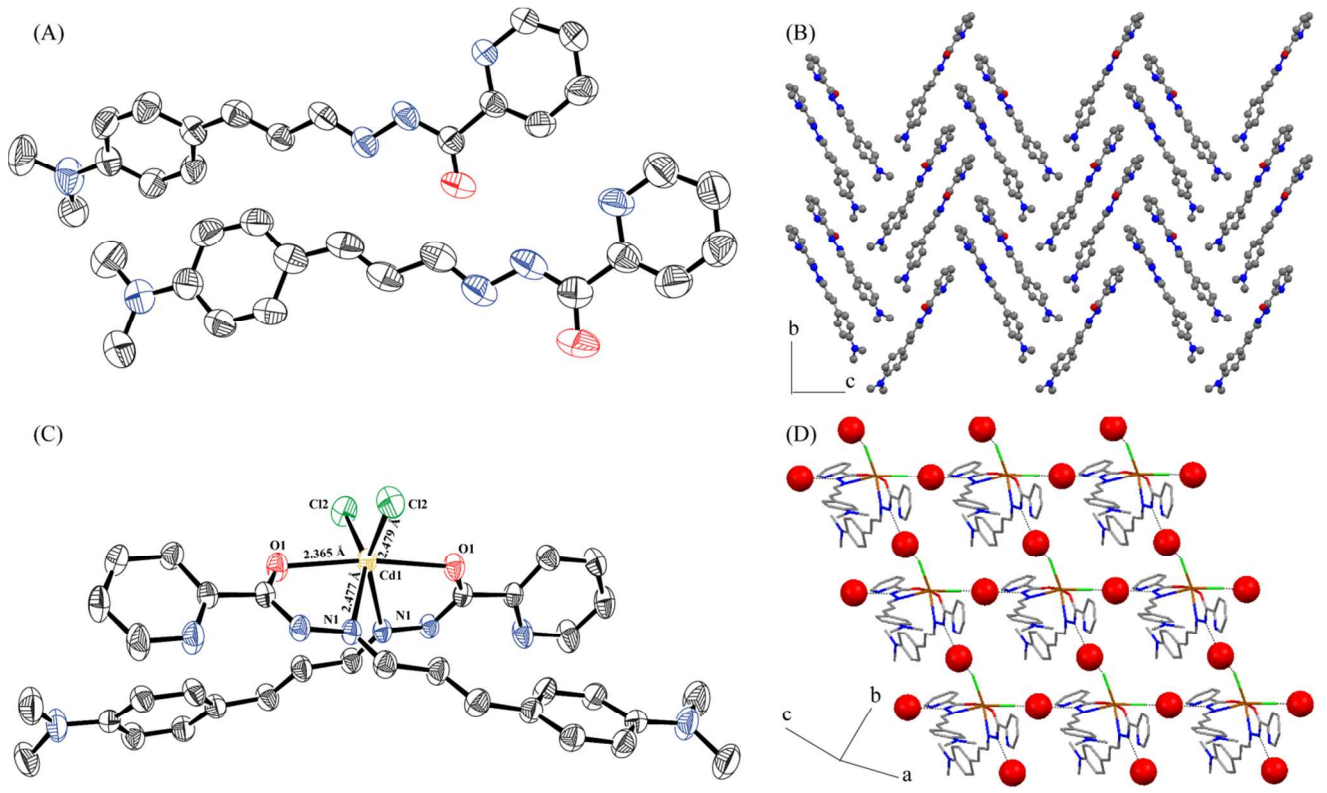

Fig. 4 (A) Thermal ellipsoid plot (50% probability level) of $\mathbf{L_1}$ (B) Packing diagram of $\mathbf{L_1}$ (C) Thermal ellipsoid plot (50% probability level) of the $\mathbf{L_1}$-**Cd** complex. (D) Packing diagram of $\mathbf{L_1}$-**Cd** complex. All hydrogen atoms were deleted for clarity.

X-ray Crystallographic Analysis

Single crystals of $\mathbf{L_1}$ suitable for XRD analysis were obtained from methanol, which crystallizes in monoclinic space group P21 with Z = 4. The asymmetric unit contains two symmetry-independent $\mathbf{L_1}$ molecules (Z′ = 2), which differ considerably in their torsions involving the conjugated aliphatic -CH=CH-CH=N- chain (Figure 4A). The solid states structure of the metal complex $\mathbf{L_1}$-**Cd** was also investigated by X-ray crystallography. Initially, we attempted to crystallize various metal salts [Chloride and nitrate salts of Cd^{2+} and Al^{3+}] with $\mathbf{L_1}$ in a variety of solvents. Indeed, the crystals suitable for crystallographic analysis were obtained in DMF/methanol mixture. The crystal structures and data of both the ligand and the complex are shown in Figure 4, and Table 1. In the Cd complex $\mathbf{L_1}$-**Cd**, each asymmetric unit contains one coordinating ligand, where Cd^{2+} is chelated by imine nitrogen, carbohydrazide oxygen, and chloride anion. Two ligand molecules along with chloride ions form disordered octahedral coordination geometry. The Cd^{2+}–N bond distance is 2.477 Å, the Cd^{2+}-Cl^- bond distance is 2.479 Å and the distance between O and Cd^{2+} is of 2.365 Å. These data demonstrate that the hydrazide moiety is mainly involved in the capture of metal ions, while the cinnamaldehyde moiety is responsible for the optical response of the sensor. From X- ray crystallographic study we found that 2:1 binding stoichiometry is favoured in solid-state, but in solution 1:1 stoichiometry is proved. The discrepancy between the binding stoichiometry in the solid-state and solution is in-lieu with the known literature.[26] However, repeated attempt to get X-ray quality crystal of $\mathbf{L_1}$-$\mathbf{Al^{3+}}$ complex was unsuccessful.

Metal-Ion Competition Studies

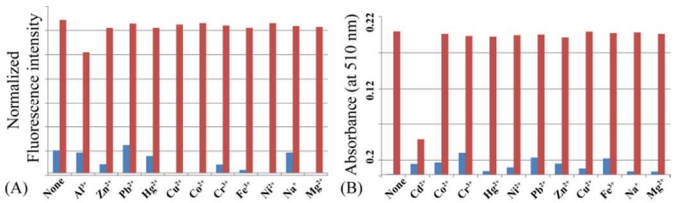

Fig. 5 (A) Normalized fluorescence responses of $\mathbf{L_1}$ (10 μM) to various cations in CH_3OH/aqueous HEPES buffer (5 mM, pH 7.3; 1:4 v/v). The blue bars represent the emission intensities of $\mathbf{L_1}$ in the presence of cations of interest (50 μM). The red bars represent the change of the emission that occurs upon the subsequent addition of Cd^{2+} to the above solution; the intensities were recorded at 578 nm. (B) Absorbance of $\mathbf{L_1}$ (10 μM) at the wavelength 510 nm in presencence of various cations in CH_3OH/aqueous HEPES buffer (5 mM, pH 7.3; 1:4 v/v). The blue bars represent the absorbance of $\mathbf{L_1}$ in the presence of cations of interest (50 μM/ 5 equivalent). The red bars represent the change of the absorbance that occurs upon the subsequent addition of Al^{3+} to the above solution.

The individual emission response of $\mathbf{L_1}$ in presence of different transition-metal ions had revealed a notable selectivity of Cd^{2+} and Al^{3+} binding (Figure 1 & 2). However, the most important criterion for a selective cation probe is the ability to detect a specific cation in a complex milieu of other competing ions. To validate this hypothesis, the selectivity of $\mathbf{L_1}$ was further tested in presence of other competing cations, which may interfere with the estimation of Cd^{2+} or Al^{3+} (figure 5A). The emission intensity of Cd^{2+}-bound $\mathbf{L_1}$ was nearly unaltered in the presence of 5 equiv of Na^+, Mg^{2+}, Cr^{3+}, Hg^{2+}, Cu^{2+}, Pb^{2+}, Zn^{2+}, Fe^{3+}, Co^{2+}, Ni^{2+} and Al^{3+}, indicating excellent selectivity for Cd^{2+} over these competing cations. The response of $\mathbf{L_1}$ for Al^{3+} over other competing metals ions was evaluated based on UV-Visible absorbance at 510 nm. It was observed that sensitivity of $\mathbf{L_1}$ towards Al^{3+} in the presence of Cd^{2+} was relatively low but presence of other metal ions did not affect the detection (figure 5B).

Application of $\mathbf{L_1}$ in Paper strips

The strong sensing potential of $\mathbf{L_1}$ for Al^{3+} and Cd^{2+} ions are further verified by incorporation in paper strips. Sensing paper strips were prepared by coating the $\mathbf{L_1}$ solution (in chloroform) on a filter paper to demonstrate the in-field device application. As evident from figure 6 paper strips coated with only $\mathbf{L_1}$ exhibited a moderate yellow emission under a hand held UV lamp. However, after dipping it into cadmium nitrate solution an intense orange fluorescence was observed. The aluminium sensing behaviour of $\mathbf{L_1}$ under visible light was also captured in a sharp change in colour of the paper strip from yellow to red. Thus, the paper strips dipped in a solution of $\mathbf{L_1}$ showed a turn on response similar to the result obtained from the spectroscopic studies and was selective to Cd^{2+} and Al^{3+}. Although zinc is known to be analogous to cadmium in spectroscopic behavior it was interesting to observe that zinc failed to promote any turn ON response neither with the paper strips, nor in the fluorescence emission studies. To the best of our knowledge this is the first report where a monomeric sensor molecule is used to demonstrate the paper strip model that can efficiently sense Cd^{2+} in presence of other metals including Zn^{2+}.

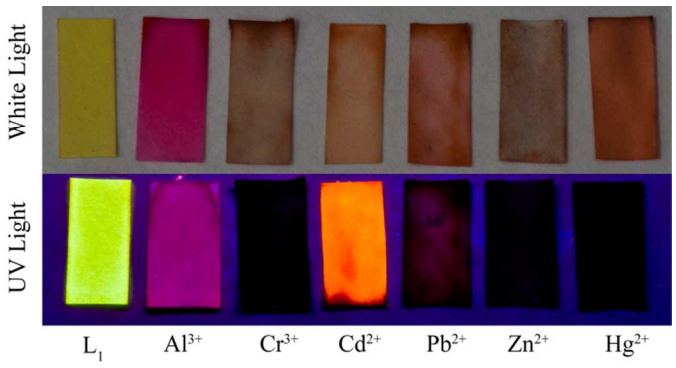

Fig. 6 Demonstration of the Al^{3+} and Cd^{2+} sensing in water by $\mathbf{L_1}$ coated (25μM solution) paper strips**.** Strength of the metal solutions used was 25μM.

Intracellular sensing of Cd^{2+} by imaging studies

Given the significant physiological and toxicological implications of cellular cadmium pool, there is considerable motivation in developing probes for detecting intracellular levels of cadmium. In our study, the results obtained in solution-based fluorescence measurements with the ligand $\mathbf{L_1}$ demonstrated the potential of the ligand to selectively detect Cd^{2+} at low levels. However, to harness the potential of the ligand $\mathbf{L_1}$ for sensing intracellular Cd^{2+} levels, it was pertinent to initially determine the cytotoxic effect of $\mathbf{L_1}$ as well as the $\mathbf{L_1}$**-Cd** complex.

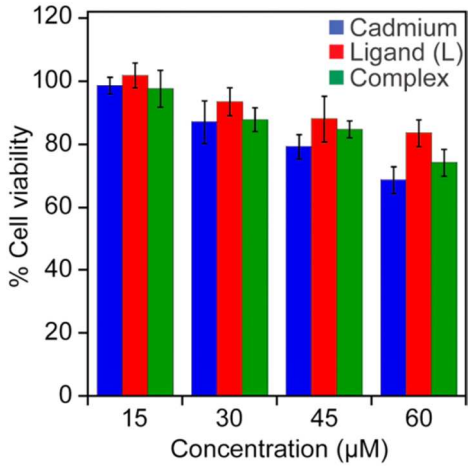

Fig. 7 MTT assay to determine the cytotoxic effect of compound $\mathbf{L_1}$ and $\mathbf{L_1}$**-Cd** complex on HeLa cells.

A standard *in vitro* MTT assay suggested that at low concentrations (upto 30μM) both $\mathbf{L_1}$ and $\mathbf{L_1}$**-Cd** complex failed to exert any detrimental effect on the viability of HeLa cells (Figure 7). The non-toxic nature of the ligand $\mathbf{L_1}$ holds significant implications in the context of sensing and suggested that the developed sensor was not only selective for Cd^{2+} but also amicable to non-destructive intracellular sensing of the metal ion. Encouraged by the non-toxic attribute of $\mathbf{L_1}$, our subsequent endeavor was to ascertain the sensing potential of $\mathbf{L_1}$ for intracellular detection of Cd^{2+} through fluorescence microscopy.

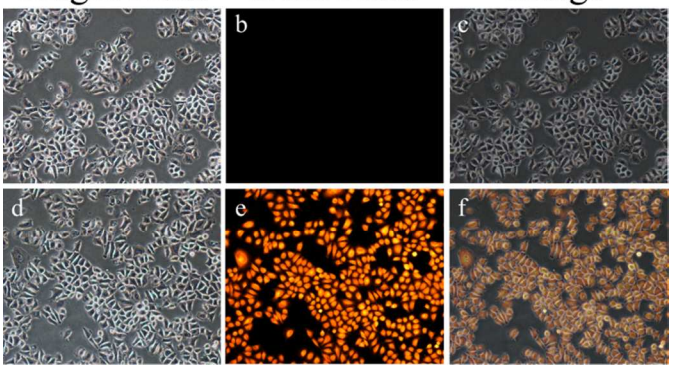

Fig. 8 Fluorescence microscopic images of HeLa cells after adding 10 μM of $\mathbf{L_1}$ (panel a-c) and after subsequent treatment with 15 μM Cd^{2+}, (panel d-f).

When HeLa cells were treated with 10 μM $\mathbf{L_1}$, the cells failed to exhibit any fluorescence (Figure 8B, Panel b). Interestingly, when the cells were subsequently exposed to 15 μM $Cd(NO_3)_2$, a dramatic switch-ON orange fluorescence manifested (Figure 8B, Panel e), indicating selective sensing of Cd^{2+} in cells. The evenly distributed intracellular fluorescence observed across HeLa cells suggested that the ligand $\mathbf{L_1}$ could transit through the membrane and pervade the cells and upon subsequent addition of $Cd(NO_3)_2$, formation of the highly fluorescent $\mathbf{L_1}$**-Cd** complex resulted throughout the cell. It was also observed that HeLa cells retained their typical morphological trait during treatment with the ligand and $Cd(NO_3)_2$ as evident from the bright field images of treated cells (Figure 7B, Panels a and d). This observation also suggested that the ligand $\mathbf{L_1}$ as well as $\mathbf{L_1}$**-Cd** complex were not cytotoxic to HeLa cells, corroborating earlier results of the MTT assay.

Conclusion

In summary, we have developed a receptor $\mathbf{L_1}$ which selectively sense Al^{3+} and Cd^{2+} ions with a switch ON response respectively in optical and fluorescence spectra in the visual region. Apart from the visible changes, an in-field device application was further demonstrated by sensing Al^{3+} and Cd^{2+} ions in paper strips coated with $\mathbf{L_1}$. Binding ability of the receptor with Cd^{2+} was confirmed by single crystal X-ray diffraction studies of the complex, which also supports the strong interaction between the ligand and Cd^{2+} ions. The fluorescence spectroscopic studies revealed that $\mathbf{L_1}$ displayed strong preference for Cd^{2+} ions over other interfering ions including Zn^{2+}. The observations of the cytotoxicity assay and fluorescence-based cell imaging are encouraging for future diagnostic applications of the sensor. Given the fact that the ligand $\mathbf{L_1}$ and $\mathbf{L_1}$**-Cd** complex were found to be non-toxic to cultured HeLa cells even after 24 h interaction period, the cadmium probe $\mathbf{L_1}$ developed in the present study holds interesting prospect in analytical and biomedical domain applications.

Acknowledgements

G.D. acknowledges CSIR (01/2727/13/EMR-II) and SERB (SR/S1/OC-62/2011) New Delhi, India for financial support, CIF, IIT Guwahati and Department of chemistry for providing instrument facilities and DST−FIST for single crystal X-ray diffraction facility. CK, SS, SG acknowledge Department of Chemistry, Central instrumental facility and IIT Guwahati for instrumental support and fellowship. We thank Department of Biotechnology, Government of India for a research grant (BT/01/NE/PS/08).

Notes and references

[a] Department of Chemistry, Indian Institute of Technology Guwahati, Assam, 781 039, India.
[b] Department of Biotechnology, Indian Institute of Technology Guwahati, Assam, 781 039, India.

Electronic Supplementary Information (ESI) available: ^{1}H NMR, ^{13}C NMR, mass spectra as characterization data of $\mathbf{L_1}$ and $\mathbf{L_1}$**-Cd** complex. Benesi-Hildebrand plot, Job's plot, UV-vis spectra and fluorescence spectra of $\mathbf{L_2}$ and $\mathbf{L_3}$, details of the result obtained from DFT calculation.

1 The European Parliament and the Council of the European Union, "Directive on the Restriction of the Use of Certain Hazardous Substances in Electrical and Electronic Equipment". 2002/95/EC.
2 W. De Vries, P. F. Romkens and G. Schutze, *Rev. Environ. Contam. Toxicol.*, 2007, **191**, 91.
3 R. R. Lauwerys, A. M. Bernard, H. A. Reels and J.-P. Buchet, *Clin. Chem. (Washington, D. C.)*, 1994, **40**, 1391.
4 G. F. Nordberg, R. F. M. Herber and L. Alessio, Cadmium in the Human Environment, Oxford University Press, Oxford, UK, 1992.
5 Agency for Toxic Substances and Disease Registry, 4770 Buford Hwy NE, Atlanta, GA 30341 http://www.atsdr.cdc.gov/cercla/07list.html.
6 a) M. E. Huston, C. Engleman and A. W. Czarnik, *J. Am. Chem. Soc.,* 1990, **112**, 7054; b) C. Lu, Z. Xu, J. Cui, R. Zhang and X. Qian, *J. Org. Chem.,* 2007, **72**, 3554; c) M. Choi, M. Kim, K. D. Lee, K.-N. Han, I.-A. Yoon, H.-J. Chung and J. Yoon, *Org. Lett.,* 2001, **3**, 3455; d) T. Gunnlaugsson, T. C. Lee and R. Parkesh, *Org. Lett.,* 2003, **5**, 4065; e) R. T. Bronson, D. J. Michaelis, R. D. Lamb, G. A. Husseini, P. B. Farnsworth, M. R. Linford, R. M. Izatt, J. S. Bradshaw and P. B. Savage, *Org. Lett.,* 2005, **7**, 1105; f) X. Tang, X. Peng, W. Dou, J. Mao, J. Zheng, W. Qin, W. Liu, J. Chang and X. Yao, *Org. Lett.,* 2008, **10**, 3653; g) L. Prodi, M. Montalti, N. Zaccheroni, J. S. Bradshaw, R. M. Izatt and P. B. Savage, *Tetrahedron Lett.,* 2001, **42**, 2941.
7 a) T. Cheng, Y. Xu, S. Zhang, W. Zhu, X. Qian and L. Duan, *J. Am. Chem. Soc.,* 2008, **130**, 16160; b) T. Cheng, T. Wang, W. Zhu, X. Chen, Y. Yang, Y. Xu and X. Qian, *Org. Lett.,* 2011, **13**, 3656; c) M. Taki, M. Desaki, A. Ojida, S. Iyoshi, T. Hirayama, I. Hamachi and Y. Yamamoto, *J. Am. Chem. Soc.,* 2008, **130**, 12564; d) W. Liu, L. Xu, R. Sheng, P. Wang, H. Li and S. Wu, *Org. Lett.,* 2007, **9**, 3829.
8 a) J. Barcelo and C. Poschenrieder, *Environ. Exp. Bot.,* 2002, **48**, 75; b) B. Valeur and I. Leray, *Coord. Chem. Rev.,* 2000, **205**, 3; c) Z. Krejpcio and R. W. P. J. Wojciak, *Environ. Studies,* 2002, **11**, 251.

9 a) G. D. Fasman, Coord. *Chem. Rev.,* 1996, **149**, 125; b) P. Nayak, *Environ. Res.,* 2002, **89**, 111; c) C. S. Cronan and W. J. Walker, P. R. Bloom, *Nature,* 1986, **324**, 140; d) G. Berthon, *Coord. Chem.Rev.,* 2002, **228**, 319; e) D. R. Burwen, S. M. Olsen, L. A. Bland, M. J. Arduino, M. H. Reid, W. R. Jarvis, *Kidney Int.,* 1995, **48**, 469.

10 a) H. M. Park, B. N. Oh, J. H. Kim, W. Qiong, I. H. Hwang, K.-D. Jung, C. Kim and J. Kim, *Tetrahedron Lett.,* 2011, **52**, 5581; b) D. Maity and T. Govindaraju, *Chem. Commun.,* 2010, 4499; c) D. Maity and T. Govindaraju, *Inorg. Chem.,* 2010, **49**, 7229.

11 a) C. R. Lohani, J.-M. Kim, S.-Y. Chung, J. Yoon and K.-H. Lee, *Analyst*, 2010, *135*, 2079; H. O. Jang, K. Nakamura, S.-S. Yi, J. S. Kim, J. R. Go and J. J. Yoon, *Inclusion Phenom. Macrocycl. Chem.,* 2001, **40**, 313.

12 J. L. Ren, J. Zhang, J. Q. Luo, X. K. Pei and Z. X. Jiang, *Analyst,* 2001, **126**, 698.

13 Y.-W. Wang, M.-X. Yu, Y.-H. Yu, Z.-P. Bai, Z. Shen, F.-Y. Li and X.-Z. You, *Tetrahedron Lett.,* 2009, **50**, 6169.

14 here in the format A. Name, B. Name and C. Name, *Journal Title*, 2000, **35**, 3523; A. Name, B. Name and C. Name, *Journal Title*, 2000, **35**, 3523.

15 C. Kar, M. D. Adhikari, A. Ramesh and G. Das, *Inorg. Chem*., 2013, **52**, 743; b) C. Kar, A. Basu and G. Das, *Tetrahedron Lett*., 2012, **53**, 4754; c) C. Kar, M. D. Adhikari, A. Ramesh and G. Das, *RSC Adv*., 2012, **2**, 9201; d) C. Kar and G. Das, *J. Photochem. Photobiol. A–Chem*., 2013, **251**, 128; e) B. K. Datta, C. Kar, A. Basu and G. Das, *Tetrahedron Lett*., 2013, **54**, 771; f) B. K. Datta, S. Mukherjee, C. Kar, A. Ramesh and G. Das, *Anal. Chem*., 2013, **85**, 8369; g) C. Kar, M. D. Adhikari, B. K. Datta, A. Ramesh and G. Das, *Sensors and Actuators B*, 2013, **188**, 1132; g) C. Kar, S. Samanta, S. Mukherjee, B. K. Datta, A. Ramesh and G.Das, *New J. Chem.,*, 2014, **DOI:** 10.1039/C4NJ00239C.

16 X. Q. Wang, Z. G. Zhao, X. L. Liu and W. J. Li, *Journal of Chemical Research*, 2010, **34**, 307.

17 N. V. Shmatkova, I. I. Seifullina and O. Y. Zinchenko, *Ukrainskii Khimicheskii Zhurnal (Russian Edition)*, 2013, **79**, 33.

18 H. A. Benesi and J. H. Hildebrand, *J. Am. Chem. Soc.* 1949, **71**, 2703.

19 SMART, SAINT, and XPREP; Siemens Analytical X-ray Instruments Inc.: Madison, WI, 1995.

20 G. M. Sheldrick, SADABS: Software for Empirical Absorption Correction; Institute fur Anorganische Chemieder Universitat, University of Gottingen: Gottingen, Germany, 1999−2003.

21 G. M. Sheldrick, SHELXS-97; University of Gottingen: Gottingen, Germany, 1997.

22 G. M. Sheldrick, SHELXL-97: Program for Crystal Structure Refinement; University of Gottingen: Gottingen, Germany, 1997.

23 L. J. Farrugia, *J. Appl. Crystallogr.*, 1997, **30**, 565.

24 a) A.D. Becke, *J. Chem. Phys.*, 1993, **98**, 5648; b) C. Lee, W. Yang and R. G. Parr, *Phys. Rev. B*, 1988, **37**, 785. c) D. Andrae, U. Haeussermann, M. Dolg, H. Stoll and H. Preuss, *Theor. Chim. Acta*, 1990, **77**, 123.

25 a) W. A. E. Omar, *J. Adv. Res.*, 2013, **4**, 525; b) F. Suzuki , T. Fukushima , M. Fukuchi and H. Kaji, *J. Phys. Chem. C*, 2013, **117**, 18809.

26 a) A. Basu and G. Das, *Dalton Trans.*, 2012, **41**, 10792; b) A. Basu and G. Das, *J. Org. Chem.*, 2014, **79**, 2647; c) J. Rebek, Jr. *Acc. Chem. Res.*, 2009, **42**, 660.

Graphical Abstract

Selective recognition of Al^{3+} and Cd^{2+} by UV-Vis and fluorescence based techniques using a cinnamaldehyde functionalized conjugated ligand and their application in paper strip and live cell imaging.